JOURNAL OF MATERIALS SCIENCE 32 (1997) 5363–5370

Characterization of a cubic phase in an Al–Cu–Mg–Ag alloy

QIONG LI and F. E. WAWNER
Materials Science Department, University of Virginia, Charlottesville, VA 22903, USA

The overall objective of this study is to investigate the microstructural stability and mechanical properties of Al–Cu–Mg–Ag alloys subjected to elevated temperatures. The addition of Ag to Al–Cu–Mg alloys with correct Cu-to-Mg ratio has been shown to generate a precipitate phase, designated Ω, which displays superior thermal stability compared with the normally occurring S′ and θ′. Samples produced for this study contained the expected Ω, θ′ and S′. In addition a cubic phase, previously designated σ($Al_5Cu_6Mg_2$), was obtained. The σ phase was seen to be a semicoherent and coplanar phase with the Al matrix, i.e., $\{100\}_\sigma // \{100\}_{Al}$ and $\langle 010\rangle_\sigma // \langle 010\rangle_{Al}$. The coarsening rate of the σ phase was found to be much lower than the θ′ phase at 200 °C. An ingot was produced of the σ phase, which was verified by X-ray diffraction. The ultrasonic technique was used to determine Young's modulus and the shear modulus. Estimates for the structural interfacial energy were determined. A hot-stage Vickers hardness measurement on the equilibrium σ phase indicates a high yield strength up to 350 °C. The data from the present study indicate that an Al alloy with the σ phase may exhibit superior elevated-temperature stability.

1. Introduction

To enhance the elevated-temperature performance of an aluminium alloy, the strengthening phases (precipitates or dispersoids) must be thermodynamically stable and resist coarsening at the temperature of interest. This is most readily achievable if the precipitate is coherent and coplanar with the matrix [1]. This correspondence implies that the precipitate–matrix interface is of a low-energy nature with little tendency for coarsening or coalescence.

Depending on the elastic misfit and interfacial energy, precipitates may assume different shapes. For example, in going from low interfacial energy and elastic strain (coherency) to high interfacial energy and large misfit (incoherency), the precipitate shape will progress through the stages of spheres, cubics, discs and needles [2]. The shape obtained is usually associated with a minimization of the total energy of particle formation. Many aluminium alloys display strengthening precipitates with needle, disc or spherical shape; however, there have been only a few observations of cubic precipitates [3–5].

Recently Schueller *et al.* [3, 4] observed a cubic precipitate which was called σ phase in a Al–Cu–Mg composite system and determined that the composition of this phase was $Al_5Cu_6Mg_2$ and has a cubic crystal structure (*Pm*3) with a lattice parameter of 0.831 nm. The orientation relationship of the precipitate with the aluminium matrix was $\{100\}_{Al} // \{100\}_\sigma$ and $\langle 010\rangle_{Al} // \langle 010\rangle_\sigma$ and the habit plane is the $\{100\}$. The edge lengths of the σ precipitate cubes were 30–50 nm. Elastic misfit between the σ phase and the aluminium matrix has been given as 2.8%, attesting to its relative coherency [4].

The objective of the present study is to characterize the σ phase with respect to microstructure, thermal stability and mechanical properties.

2. Experimental procedure

The experimental alloys were produced in the University of Virginia Materials Science Department. An induction furnace was used to melt the metallic charges. The crucible was placed in a glove-box for producing the alloys in an Ar atmosphere. After casting, all alloys were hot rolled and then homogenized for 24 h at 495 °C, solutionized for 19 h at 525 °C, quenched in ice–water and artificially aged at the different times and temperatures. An equilibrium σ phase ($Al_5Cu_6Mg_2$) was produced in the same apparatus and annealed for homogenization in an Ar atmosphere at 620 °C for 211 h and then furnace cooled. Transmission electron microscopy (TEM) was used to investigate the microstructure of the alloys. A Philips EM 400T energy-dispersive-spectroscopy-equipped analytical transmission electron microscope and a JEOL 4000EX high resolution transmission electron microscope were applied in this study. The modulus measurement of the σ phase was carried out in a laser ultrasonic apparatus. Hot-stage hardness test equipment was used to measure the hardness of the intermetallic σ phase versus temperature. Differential scanning calorimetry (DSC) (Perkin–Elmer DSC7) was used to investigate the precipitation process.

0022–2461

3. Results and discussion

Since both the σ phase and Al are cubic structures and have a crystallographic relationship $\{1\,0\,0\}_{\sigma}//\{1\,0\,0\}_{Al}$ and $\langle 0\,1\,0\rangle_{\sigma}//\langle 0\,1\,0\rangle_{Al}$, the σ phase could have a slow coarsening rate. A cube-on-cube interface is the ideal structure for use in a high-temperature application. The cube-on-cube relationship correspondence means that the precipitate–matrix interface is a low-energy interface and there is little tendency for coarsening or coalescence to reduce its interfacial energy [6]. A good example of a precipitate with cube-on-cube relationship is γ′ (Ni_3Al) in the Ni-based superalloys. The Ni-based superalloys which are used at high temperatures (up to 0.75 T_m) depend upon the presence of γ′ precipitates. They are thermodynamically stable at high temperatures. Hence what are needed for a good ductile aluminium-based alloy which would be useful above 200 °C are stable precipitates with a cube-on-cube relationship [1]. The σ phase is semicoherent and has a cube-on-cube orientation relationship with the aluminium matrix, which offers potential to achieve this goal.

TABLE I Comparison of the studied alloys

Alloy	Amount (wt%) of the following elements			
	Cu	Mg	Ag	Al
A11M	3.2	0.45	0.4	Balance
A12M	4.0	0.45	0.4	Balance

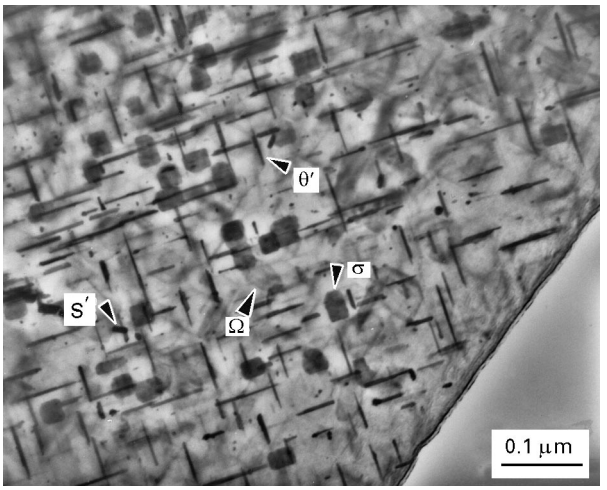

Figure 1 TEM image along the ⟨0 0 1⟩ direction showing the cubic σ phase. Other precipitates includes Ω, θ′ and S′ phases.

The compositions of the alloys studied are given in Table I.

The cubic Al–Cu–Mg phase was identified originally by Samson [7] and was determined to have the chemical formula $Al_5Cu_6Mg_2$. It has a cubic crystal structure (*Pm*3) with a lattice parameter of 0.831 nm [7]. This σ phase has not been identified in aluminium-based materials until recently. These observations demonstrated that the cubic phase (designated σ) can be formed in Al–Cu–Mg–Ag and Al–Cu–Mg–Si alloys as second major precipitate. Fig. 1 shows the general appearance of the σ phase along the ⟨0 0 1⟩ direction coexisting with other phases expected for this alloy. The sample was aged at 200 °C for 3 h. Fig. 2 shows the electron diffraction patterns which display several orientation relationships of σ and matrix. All directions show the σ phase to be coplanar with the Al matrix. Fig. 3 is a high-resolution micrograph showing the semicoherent interface of the σ phase and Al matrix. Owing to the overlap of and difference between the lattice parameters of the σ phase and Al matrix, Moiré fringes formed in the image.

To confirm the identification and cube-on-cube relationship, computer-simulated selected-area diffraction patterns were constructed of the $Al_5Cu_6Mg_2$ phase in an aluminium matrix [8]. Fig. 4 shows the simulated ⟨0 0 1⟩, ⟨0 1 1⟩, ⟨1 1 2⟩ and ⟨1 1 1⟩ patterns, which are seen to match well with that taken from the σ phase (Fig. 2). Low-index planes of σ phase and Al matrix are matched well, which suggests that the cube-on-cube relationship is satisfied.

The misfit between the σ phase and matrix is 2.57% (assuming that $a_{Al} = 0.405$ nm) which is slightly lower than 2.8% ($a_{Al} = 0.404$ nm) reported in the literature [4]. Because the misfit is small, a strain field can be built up near the interface region and give rise to strain

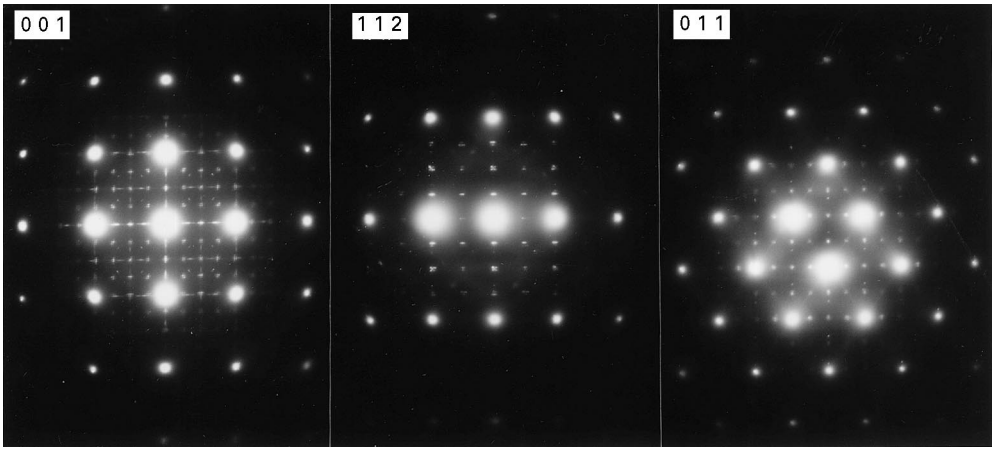

Figure 2 Electron diffraction patterns of the σ phase and Al matrix in the ⟨0 0 1⟩, ⟨1 1 2⟩ and ⟨0 1 1⟩ directions.

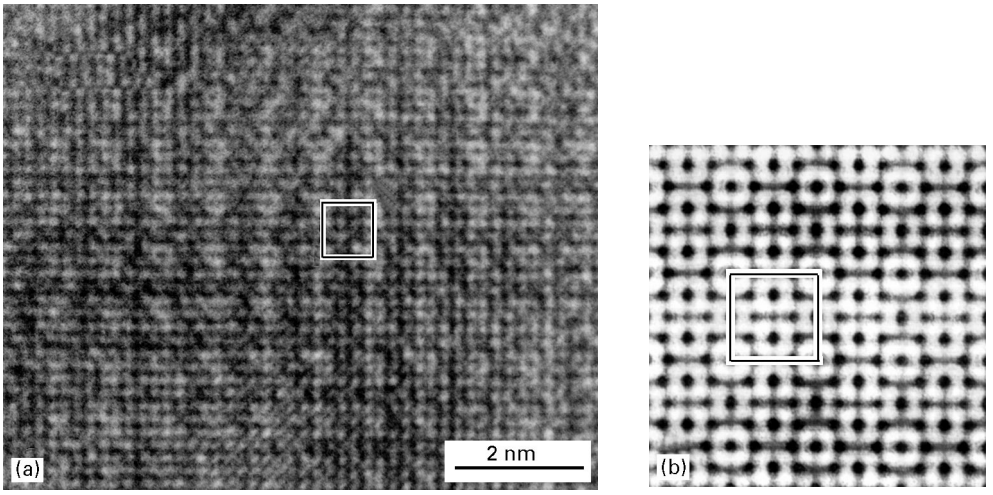

Figure 3 (a) High-resolution TEM image of the σ phase along $[0\,0\,1]_{Al}$ and (b) its image simulation. Both images show a two-fold symmetry.

contrast. Fig. 5 shows that the strain field is depicted as periodic lobes in the matrix near the interface. The spacing was measured from the transmission electron micrograph to be between 7.0 and 8.0 nm which is smaller than the measurement (12–13 nm) made by Schueller *et al.* [4]. However, the composition of the material used in this study was different from the work by Schueller *et al.* The difference between the misfit dislocation spacings in the σ phase for these two materials suggest that the coherence of the σ phase could be adjusted by adding different solute elements, which is similar to γ′ in Ni-based superalloys.

The TEM results indicate that the alloy with a Cu-to-Mg ratio of about 7 forms more σ phase than that with a Cu-to-Mg ratio of about 10. Fig. 6 shows a high density of the σ phase in the alloys. Other phases can also be seen in the micrograph. The θ′ and S′ phases appear as plate edge and needle shape and parallel to the $\{1\,0\,0\}$ aluminium planes; the Ω phase which is formed on $\{1\,1\,1\}$ planes is inclined in this orientation [9]. The Cu-to-Mg ratio and the Ag addition are important for the formation of the Ω and σ phases. The previous study on the σ phase indicates that Si acts as a nucleation agent [10]. In this Al–Cu–Mg–Ag alloy the Ag could play the same role as Si in the (Al–Cu–Mg)–SiC whisker metal matrix composite [3]. The Ag addition increases Ω phase formation in the high-Cu-to-Mg-ratio alloy and σ phase formation in the low-Cu-to-Mg-ratio alloy. One of the unique properties of the σ phase is that it is an equilibrium phase with a high melting temperature (710 °C) [7]. This implies the Al alloy strengthened by the σ precipitates will have thermodynamic stability at elevated temperatures.

3.1. Mechanical properties of the σ phase

Since the σ phase is an equilibrium phase, a sample was cast as previously described to evaluate its mechanical properties. The composition of the intermetallic compound was confirmed by X-ray diffractometry. Young's modulus, E, the shear modulus, G, and Poisson's ratio, ν, were determined by ultrasonic techniques. These measurements gave a value of 160 GPa for E, 61 GPa for G and 0.308 for ν (see Appendix A). Hardness tests at room temperature were made on this material displaying a high value of hardness (Vickers hardness, 546 $kg\,mm^{-2}$). Because this intermetallic compound is extremely brittle, there is no work hardening; hence the yield strength can be calculated as one third of the Vickers hardness [11]. This gives a yield strength, σ_y, for the σ phase of 1784 MPa. Hot-stage hardness tests (Fig. 7) show that the intermetallic material retained 70% of its room temperature value at 350 °C.

3.2. Interfacial energy of the σ phase

The interfacial energy, γ, is one of the important parameters for the precipitation process; for instance, for the nucleation barrier, $G^* \propto \gamma^3/(G_v + w)^2$ and, for the coarsening of precipitates, $r^3 \propto \gamma t$. In general the interfacial energy γ between two solid phases can be split into two components:

$$\gamma = \gamma_{struct} + \gamma_{chem}$$

The structural interfacial energy of the σ phase was calculated by using the van den Merwe model [12] which considers an array of misfit dislocations contribution to the interfacial energy. The basic parameters such as E, G and ν needed for calculations used in the model were determined above. The spacing between misfit dislocations was measured from transmission electron micrographs. Since there is a small misfit between the σ phase and the matrix of 2.57%, the misfit dislocations can build up a periodic strain near the interface region. Fig. 5 show the periodic lobes caused by misfit dislocation strain in the matrix near the interface. The misfit dislocation spacing, p, is about 7.0 nm; here the spacing of the strain lobes is considered the misfit dislocation period. Using this approach, the interfacial energy of the σ phase was calculated as 0.0111 $J\,m^{-2}$ (see Appendix B).

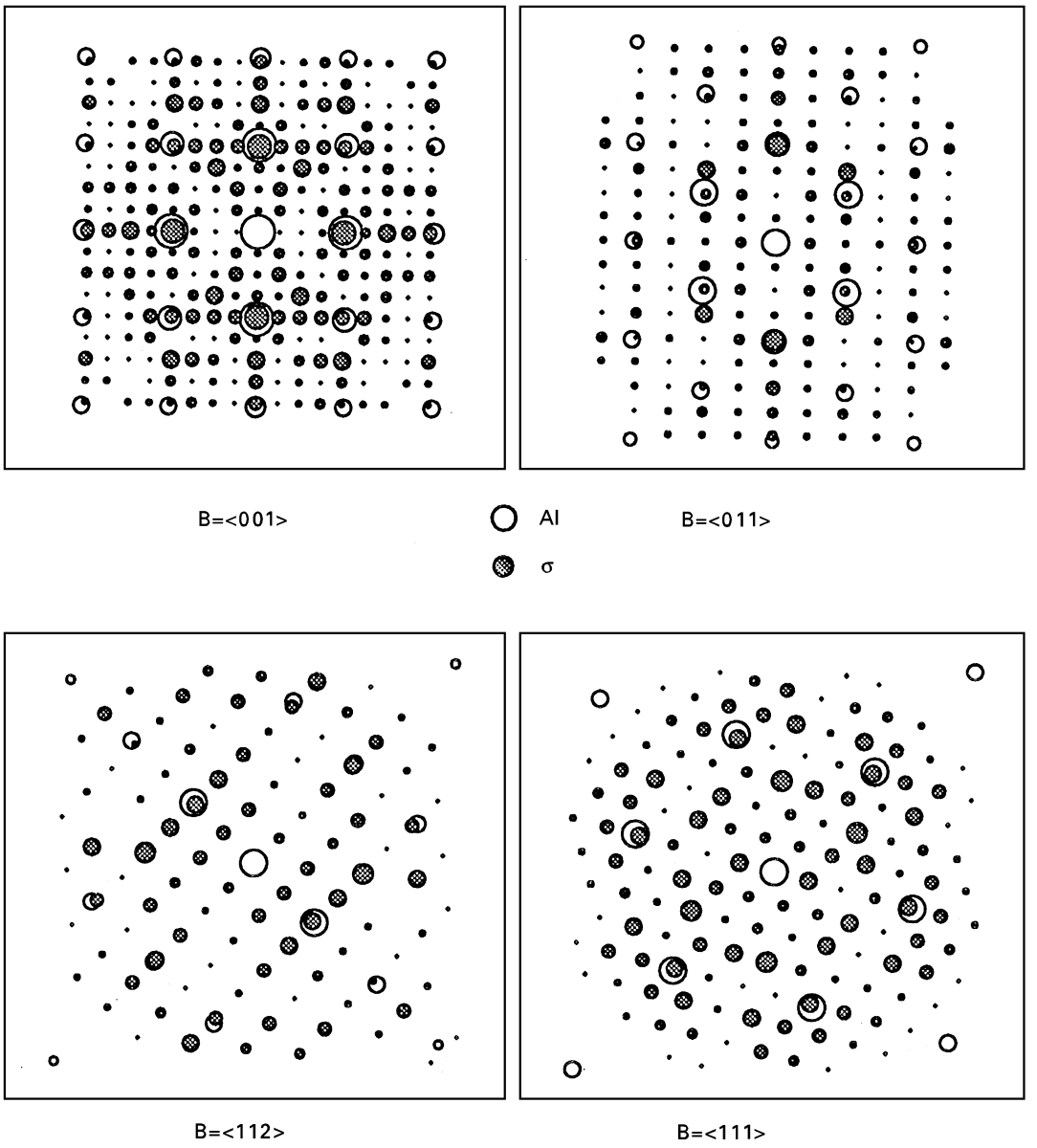

Figure 4 Computer simulation of diffraction pattern for the σ phase in the Al matrix.

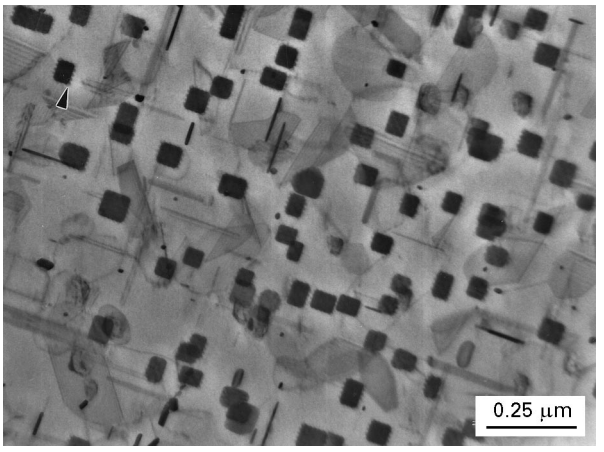

Figure 5 Strain lobes formed near the interface in the matrix, which is due to the misfit between the σ and Al. The period of the lobe is about 7.0 nm.

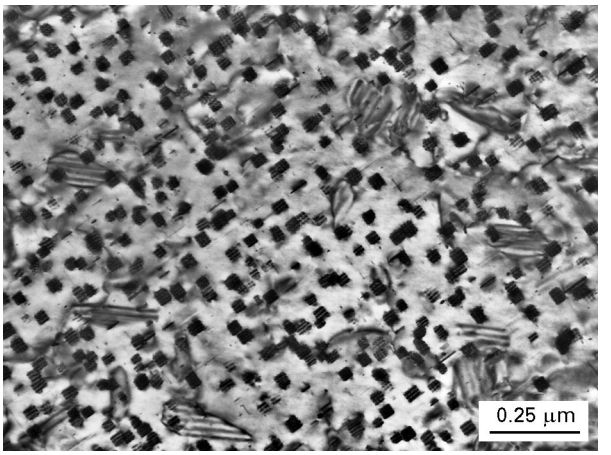

Figure 6 The high density of the σ phase in the alloys.

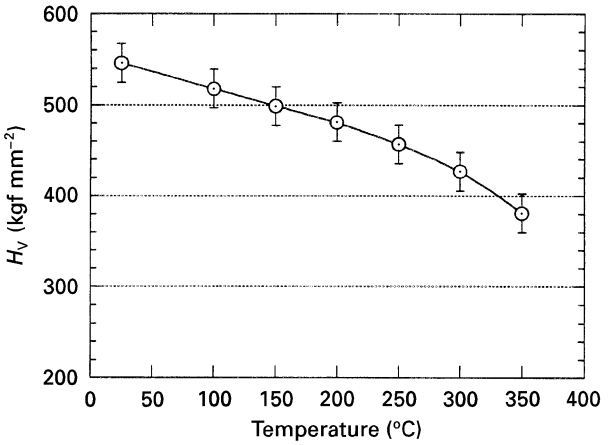

Figure 7 The Vickers hardness, H_v, of σ phase as a function of testing temperature.

The chemical term of the interfacial energy can be estimated using a broken-bond model [13, 14]. Considering only the nearest-neighbour interaction

$$\gamma_{chem} = \frac{E(\text{Al–Al})}{\text{unit area}} - \frac{E(\text{Al–s})}{\text{unit area}}$$

Consider the major contribution to the chemical term is the enthalpic component which arise from the excess energy of the bonds across the interface:

$$\Delta H_{ex} = H_{Al\text{–}Cu} - 0.5(H_{Al\text{–}Al} + H_{Cu\text{–}Cu})$$

where ΔH_{ex} is the excess chemical energy, and $H_{Al\text{–}Cu}$, $H_{Al\text{–}Al}$ and $H_{Cu\text{–}Cu}$ are the binding energy of Al–Cu, Al–Al and Cu–Cu, respectively. The bond energy, $\varepsilon_{Al\text{–}Cu}$, between Al and Cu atoms can be obtained from the Bragg–Williams [15] approximation:

$$0.25 k_B T_c = \varepsilon_{Al\text{–}Cu} - 0.5(\varepsilon_{Al\text{–}Al} - \varepsilon_{Cu\text{–}Cu})$$

where T_c is the critical ordering temperature which can be extrapolated from phase diagram. The Al–Al and Cu–Cu bond energies can be estimated from the heat of sublimation of the pure metal, ΔH_s:

$$\Delta H_s = \frac{\Delta H_e}{N_A N_B}$$

where N_A is the Avogadro constant and N_B is the number of nearest neighbours. Using these relationships, the chemical contribution to the interfacial energy is finally calculated as [16]

$$\gamma_{chem} = 0.0128 \text{ J m}^{-2}$$

The total interfacial energy between σ and aluminium is

$$\gamma = \gamma_{struct} + \gamma_{chem} = 0.0111 + 0.0128 = 0.0239 \text{ J m}^{-2}.$$

Comparing the σ phase in aluminium with the $\gamma'(Ni_3Al)$ phase in the Ni-based superalloys it can be seen that they are both cubic phases and have semicoherent, coherent and cube-on-cube orientation relationships with their matrix, they have close values of interfacial energy, namely 0.0239 J m^{-2} for the σ phase and 0.014 J m^{-2} for the γ' phase, and they are both stable at elevated temperatures [3].

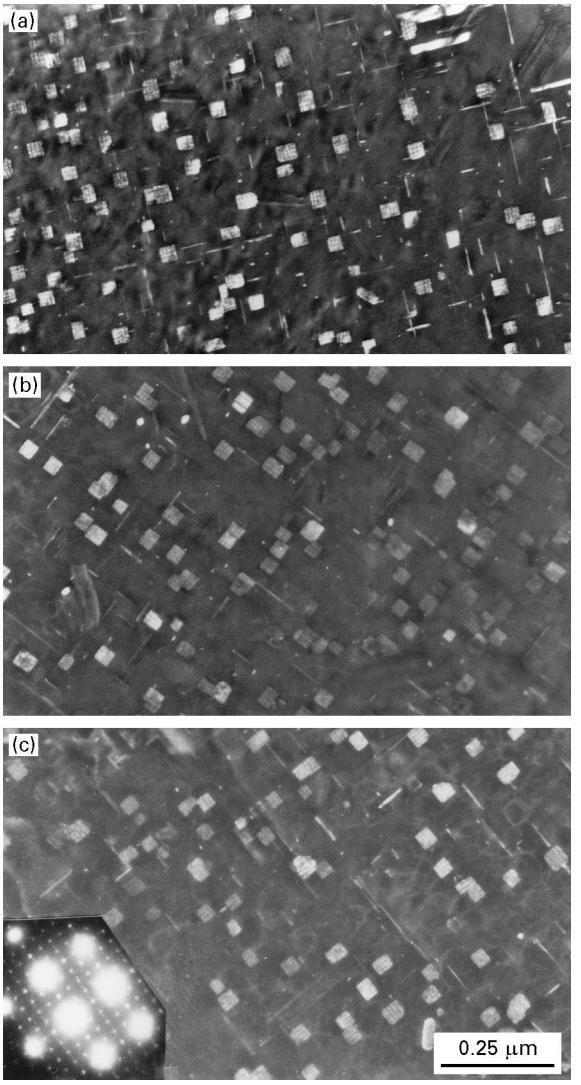

Figure 8 The σ phase size as a function of exposure time at 200 °C: (a) 26.2 h; (b) 100 h; (c) 405 h.

3.3. Growth rate of the σ phase

A particle size analysis was carried out on the σ phase precipitates aged at 200 °C for different times. The transmission electron micrographs in Fig. 8 show that there is very little size change of the σ phase. After exposure for more than 400 h at 200 °C, the σ phase still remains in a high density in the alloy, and the diffraction pattern shows strong σ-phase reflections. The size of the σ phase was determined by measuring over 200 precipitates for each ageing condition and then plotting the mean value of the size as function of time. Fig. 9 is the plot of average precipitate size versus time. The graph shows that the average size of the σ phase increases at a very slow rate after a certain size is formed. The graph displays the large difference between the sizes and coarsening behaviour between the σ and θ′ phases [17]. The relationship of the maximum size of the σ phase versus exposure time at 200 °C (Fig. 10) indicates a slow coarsening rate, which follows a power law $r \propto t^{1/5.6}$, compared with $t^{1/3}$ for the Lifshitz–Slyozov–Wagner (LSW) theory prediction.

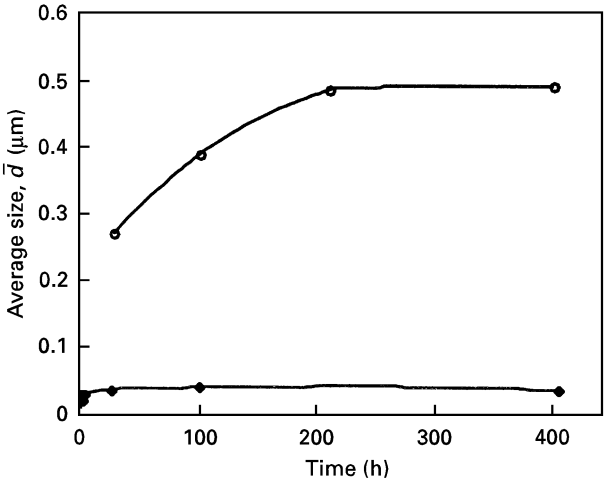

Figure 9 Comparison of the size of the σ phase (●) and the θ′ phase [17] (○) at 200 °C exposure.

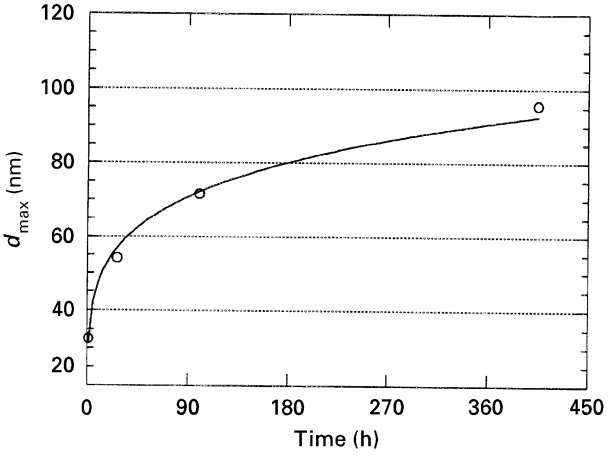

Figure 10 Coarsening behaviour of the σ phase at 200 °C. (—), $y = 31.829x^{0.177\,83}$, $R = 0.996\,62$.

Observations of ledge morphology indicate that the σ phase has a straight ledge and fewer growth ledges than the other phases. Two kinds of ledge were observed by TEM: a straight ledge and a ledge with kinks. When a ledge has a straight facet step, the ledge migrates with great difficulty [18]. For a ledge with kinks, as the kinks filled, the ledge becomes a straight facet configuration. The transmission electron micrographs in Fig. 11a and b show a ledge with kinks and a straight ledge configuration respectively. The slow coarsening rate is due to the low interfacial energy of the σ phase and the few straight growth ledges on the σ phase. The result is consistent with the prediction that precipitates with coherent interfaces, low interfacial energy and few growth ledges have a slow growth rate. A statistical analysis of size distribution (Fig. 12) shows the size distribution of the σ phase and comparison with LSW coarsening theory prediction. The solid line in each figure represents the quasi-steady-state distribution predicted by the LSW theory of Ostwald ripening and given by the function $f(r, t) = g(t)\rho^2 h(\rho)$ [19] where $g(t)$ is a function of time only, $\rho = r/\bar{r}$, and $h(\rho)$ is given by

$$h(\rho) = \left(\frac{3}{\rho + 3}\right)^{7/3}\left(-\frac{\frac{3}{2}}{\rho - 3/2}\right)^{11/3}\exp\left(\frac{\rho}{\rho - \frac{3}{2}}\right) \quad \text{when } \rho < \tfrac{3}{2}$$

$$h(\rho) = 0 \quad \text{when } \rho > \tfrac{3}{2}$$

Of the distributions shown, none of them obeys the LSW distribution which predicts a rapid decrease in the number of particles at sizes greater than the most probable size. The distribution shows that the size of the σ phase is uniform and the most probable size is

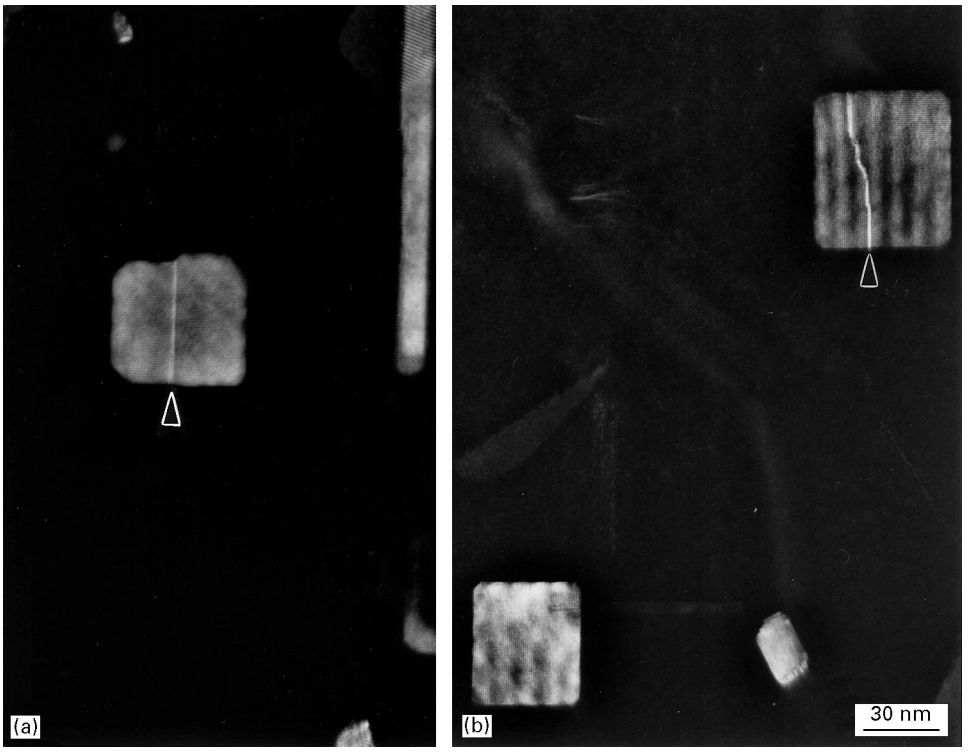

Figure 11 Ledge structures in the σ phase: (a) a straight ledge; (b) a ledge with kinks.

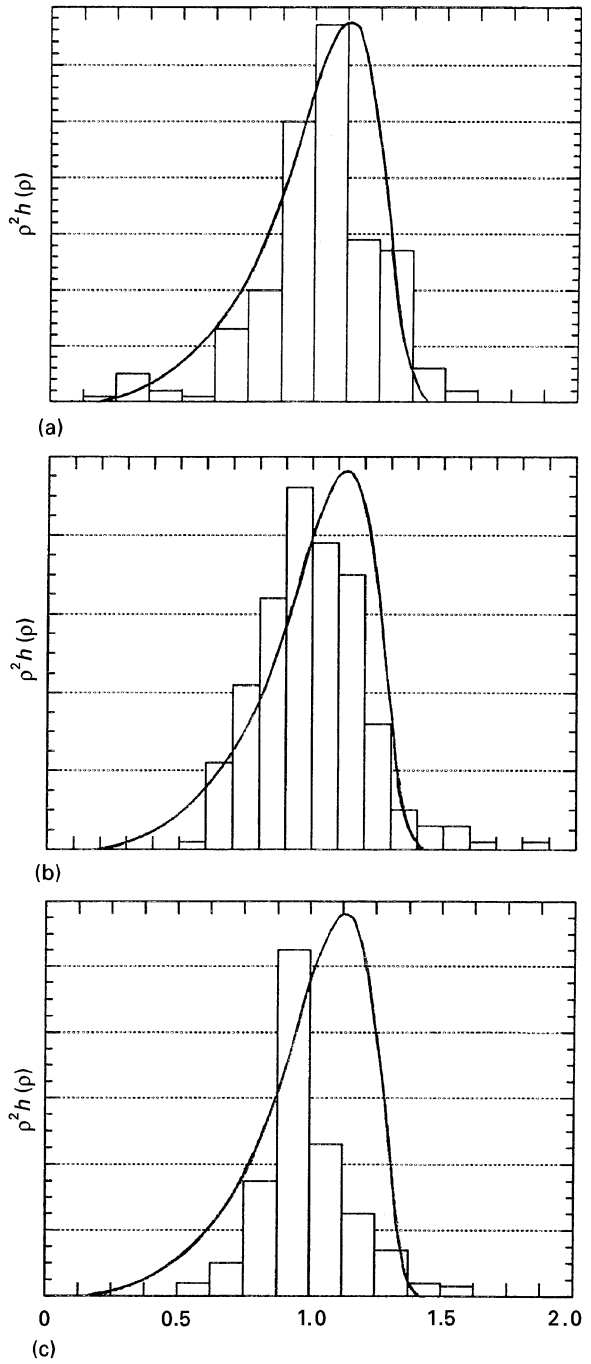

Figure 12 The size distributions of the σ phase at 200 °C for different times. (a) $t = 26.2$ h, $n = 223$; (b) $t = 100$ h, $n = 239$; (c) $t = 405$ h, $n = 247$. The solid curves are the LSW theory prediction.

smaller than the LSW theory prediction. It should be noted that the LSW theory is for the coarsening of spherical particles. The small size, narrow size distribution and very low coarsening rate of the σ phase could promote thermal stability and high mechanical properties in the alloy at elevated temperatures.

4. Conclusions

The properties of the σ phase are summarized as follows.

1. A relatively high density of the σ phase was found in Al–Cu–Mg–Ag alloy; the σ phase is semi-coherent and has a cube-on-cube orientation relationship with the aluminium matrix.

2. Young's modulus, the shear modulus and Poisson's ratio for the intermetallic σ phase were measured to be $E = 159.3$ GPa, $G = 60.89$ GPa and $\nu_\sigma = 0.308$, respectively.

3. Based on the van der Merwe model and a broken-bond model, the interfacial energy of the σ phase is calculated as $\gamma = 0.024\ \mathrm{J\,m^{-2}}$.

4. The σ phase possesses a small size and narrow size distribution at 200 °C ageing temperature. A very slow coarsening rate of the σ phase was found at 200 °C, which implies that the Al alloys strengthened by the σ precipitate phase could be stable at elevated temperatures.

5. The low coarsening rate of the σ phase is due to its low interfacial energy, small and faceted growth ledges and cube-on-cube orientation relationship.

Appendix A

E and G measurement (ultrasonic technique) give the following values:

$V_L = 6.216\ \mathrm{mm\,\mu s^{-1}} \qquad V_T = 3.270\ \mathrm{mm\,\mu s^{-1}}$

$\rho = 4.90\ \mathrm{g\,cm^{-3}}$

$$V_T = \frac{\mu^{1/2}}{\rho} \quad \frac{\mu}{\rho} = V_T^2 = 10.693\ \mathrm{mm^2\,\mu s^{-2}}$$

$\mu = 52.4$ GPa

$$E = 2G(1+\nu) \quad \frac{2^{1/2}(1-\nu)}{1-2\nu} = \frac{V_L}{V_T} = 1.901 \quad \nu = 0.308$$

$$E = 2G(1+\nu) = 137.1\ \mathrm{GPa} \quad E = \frac{E_0}{\exp^{(-pb)}}$$

$p = 0.05$ (porosity percentage)
$b = 3$ (empirical constant)
$E_0 = 159.3$ GPa $\quad G_0 = 60.89$ GPa

$E = 137$ GPa $\quad G = 52.408$ GPa

Appendix B

Calculation of the interfacial energy for the σ phase by the van der Merwe model is as follows (Table BI):

$$\gamma = \frac{GC}{4\pi^2}\,1 + \beta - (1+\beta^2)^{1/2} - \beta \ln[2\beta(1+\beta^2)^{1/2} - 2\beta^2] \tag{B1}$$

$$\beta = \frac{2\pi G_\sigma b}{p[(1-\nu_\sigma) + (1-\nu_{Al})G_\sigma/G_{Al}]G} \tag{B2}$$

$$C = \frac{a_1 + a_2}{2}$$

$$p = \frac{(a_1+a_2)^2}{4(a_1-a_2)}, \quad \text{the spacing between misfit dislocations} \tag{B3}$$

$\nu_\sigma = 0.308 \quad \nu_{Al} = 0.33 \quad b = 2$ Å

$a_1 = 2.0775$ Å $\quad a_2 = 2.025$ Å

$$G_{Al} = 27\ \mathrm{GPa} \quad G_\sigma = 61\ \mathrm{GPa} \quad G = \frac{G_{Al} + G_\sigma}{2}$$

TABLE BI Values of γ for two values of β and p

γ (J m^{-2})	β	p (Å)
0.0126	0.113	70 (measured from transmission electron micrograph)
0.0111	9.87×10^{-2}	80 (calculated from Equation 3)

Acknowledgements

The authors are pleased to acknowledge the support of National Aeronautics and Space Administration Langley Research Center, under grant NAG-1-745, contract monitors D. L. Dicus and W. D. Brewer. The authors also thank Dr Y. C. Lu for assisting with the ultrasonic equipment and Dr H. Koenigsmenn for assisting with the hot-stage hardness measurement.

References

1. M. E. FINE, in "Dispersion strengthened aluminium alloys", edited by Y. -W. Kim and W. Griffith (Minerals, Metals and Materials Society, Warrendale, PA, 1988) pp. 103–21.
2. E. A. STARKE JR, Treatise on Material Science Technology vol. 3 (1988) 35.
3. R. SCHUELLER, A. K. SACHDEV and F. E. WAWNER, *Scripta Metall.* **27** (1992) 617.
4. R. SCHUELLER, A. K. SACHDEV and F. E. WAWNER, *Scripta Metall.* **27** (1992) 1289.
5. J. E. Hatch (ed.), "Aluminium properties and physical metallurgy", (American Society for Metals, Metals Park, OH, 1984).
6. M. E. FINE, D. L. BOURELL, Z. ELIEZER, C. PERSAD and H. L. MARCUS, *Scripta Metall.* **22** (1988) 907.
7. S. SAMSON, *Acta Chem. Scand.* **3** (1949) 809.
8. "Diffract program", version 1.2, distributed by Microdev Software.
9. I. POLMEAR, *Trans. Metall. Soc. AIME* **230** (1964) 1331.
10. R. SCHUELLER, F. E. WAWNER and A. SACHDEV, *J. Mater. Sci.* **29** (1994) 424.
11. M. F. ASHBY and D. R. H. JONES, *Engng Mater.* **1** (1980) 105.
12. G. J. SHIFLET, *Mater. Sci. Engng* **81** (1986) 61.
13. D. A. PORTER and K. E. EASTERLING, "Phase transformations in metals and alloys" (Chapman & Hall, London, 2nd Edn, 1992).
14. D. E. STEPHENS and G. R. PURDY, *Acta Metal.* **23** (1975) 1343.
15. W. L. BRAGG and E. J. WILLIAMS *Proc. R. Soc. A* **145** (1934) 699.
16. Q. LI, PhD thesis, University of Virginia (1995).
17. J. D. BOYD and R. B. NICHOLSON, *Acta Metall.* **19** (1971) 1379.
18. W. T. REYNOLDS JR, Unpublished data, Virginia Polytechnical Institute.
19. M. S. ZEDALIS and M. E. FINE, *Metall. Trans. A* **17** (1986) 2187.

Received 8 October 1996
and accepted 1 May 1997